F1000Research

Check for updates

RESEARCH ARTICLE

New insights about the serine/threonine protein kinase substrates from *Mycobacterium tuberculosis* using molecular docking, quantum similarity analysis and DFT calculations [version 1; peer review: 1 approved]

Alejandro Morales-Bayuelo [iD][1], Jesús Sánchez-Márquez[2]

[1]Centro de Investigación de Procesos del Tecnológico Comfenalco (CIPTEC), Fundación Universitaria Tecnológico Comfenalco, Programa de Ingeniería Industrial, Cartagena de Indias, Colombia
[2]Departamento de Química-Física, Facultad de Ciencias, Campus Universitario Río San Pedro, Universidad de Cádiz, Cádiz, Spain

Abstract

Background: The protein kinases present in the human body have received a lot of attention because of the interest in their use as therapeutic targets. However, little is known about the protein kinases associated with tuberculosis. For these reasons, this research investigates a new point of view regarding the crystallized serine/threonine protein kinases Pkn A, B and G of *Mycobacterium tuberculosis*.

Methods: The conformational analysis shows a DFG-in motif in Pkn B and G and a DFG-out motif in Pkn A. For all the protein kinases that have been studied, the gatekeeper residue is methionine. A study of the protein kinases with their ligands was also conducted to find new insights on the binding site with a series of ligands associated to protein kinases Pkn A, B and G through molecular docking. The residues with hydrogen bonds on the hinge zone of Pkn A are GLU96 and VAL 98, of Pkn B are GLU 93 and VAL 95 and of Pkn G are GLU233 and VAL235.

Results: The results show the H-bond acceptor and H-bond donor sites on the hinge zone to all ligands, establishing a structural model of the ligands on the active site with two or three interactions in this zone. This interaction model was validated using density functional theory calculations (by means of net charges and images of the electrostatic potential) and molecular quantum similarity analysis, showing a high correlation between the electronic and steric effects in each ATP complex studied.

Conclusions: In this work we can see that the interactions of the hinge zone are characterized by the key factor of one or two H-bonds acceptors and one H-bond donor in the ligands of this zone. The quantum similarity analysis shows good correlation between the

Open Peer Review

Approval Status ✔

	1
version 1 03 Feb 2021	✔ view

1. **Hugo Fraga**, Faculdade de Medicina da Universidade do Porto - FMUP, Porto, Portugal

Any reports and responses or comments on the article can be found at the end of the article.

steric and electronic effects in each ATP complex.

Keywords

Mycobacterium tuberculosis, Serine/Threonine Protein Kinases A, B, G, Molecular Docking, Molecular Quantum Similarity Analysis, Electrostatic Interactions.

This article is included in the Chemical

Information Science gateway.

Corresponding authors: Alejandro Morales-Bayuelo (alejandr.morales@uandresbello.edu), Jesús Sánchez-Márquez (jesus.sanchezmarquez@uca.es)

Author roles: Morales-Bayuelo A: Conceptualization, Formal Analysis, Investigation, Methodology; **Sánchez-Márquez J**: Conceptualization, Formal Analysis, Investigation

How to cite this article: Morales-Bayuelo A and Sánchez-Márquez J. **New insights about the serine/threonine protein kinase substrates from *Mycobacterium tuberculosis* using molecular docking, quantum similarity analysis and DFT calculations [version 1; peer review: 1 approved]** F1000Research 2021, **10**:66 https://doi.org/10.12688/f1000research.28078.1

First published: 03 Feb 2021, **10**:66 https://doi.org/10.12688/f1000research.28078.1

Introduction

Protein kinases (PKs) are a key in controlling proliferation and differentiation in eukaryotic cells in living organisms. They are enzymes that catalyze the protein phosphorylation process. An important reason to analyse the protein phosphorylation process is that it represents an attractive drug target in a variety of fatal diseases such as cancer[1]. The PKs present in the human body have been widely used in the field of drug design because they play an important role as therapeutic targets in these diseases. However, little is known about the serine/threonine protein kinases (STPKs) involved in tuberculosis. For this reason, we propose a study about crystalized STPKs Pkn A, B and G, to gain new insights in the mechanism of the phosphorylation process.

To date, one of the main questions in the tuberculosis field is 'what are the protein substrates of the STPKs?' According to Av-Gay et al.[2], to deal with this topic we need to study the interactions of crystalized STPKs Pkn A, B and G with a particular series of ligands to each PK. The competitive ATP ligands used are a series of compounds for Pkn A reported by Sipos et al.[3], ligands for Pkn B reported by Székely et al.[4], Loughheed et al.[5] and Chapman et al.[6] and ligands for Pkn G reported by Sipos et al.[3] and Pato et al.[7]. These ligands were selected with the goal of finding new insights into the inhibition of oxidative phosphorylation. Therefore, we are researching new pharmacological alternatives for this disease through the structural models of the ligands on the ATP sites.

Another aim of this study is to conduct molecular quantum similarity (MQS) analysis using a quantum similarity field to understand the electronic and structural patterns involved in stabilization of the active site of the inhibitors for each PK studied. Therefore, a hybrid quantum mechanics/molecular mechanics (QM/MM) approach was used to carry out a structure-activity relationship analysis of the inhibitor set for Pkn A, Pkn B and Pkn G.

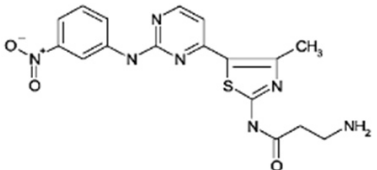## Methods

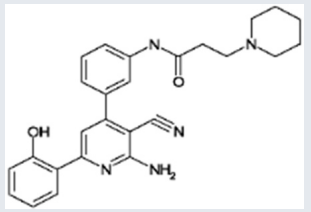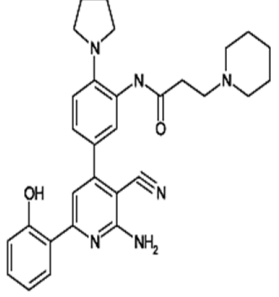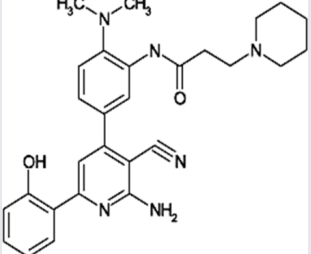### Pkn A, B and G: docking of their ATP-competitive inhibitors

The crystal structures of Pkn A (PBD code: 4OW8, resolution: 2.03 Å[8]), Pkn B1 (PDB code: 3F69, resolution: 2.80 Å[9(a)]), Pkn B2 (PDB code: 1MRU, resolution: 3.0 Å[9(b)]), Pkn B3 (PDB code: 2FUM, resolution: 2.89 Å[9(c)]) and Pkn G (PBD code: 2PZI, resolution: 2.40 Å[10]) were selected for the preparation process using Schrödinger Suite 2014-1's Protein Preparation Wizard module[11], which refines the protein structure and optimizes the hydrogen bond (H-bond) network. The open-source software AutoDock Vina could also be used to perform these steps.

Protonation states were identified using PropKa utility at a physiological pH[12]. After, restrained molecular minimization using the Impact Refinement (Impref) module[13] was carried out, taking into account the heavy atoms restrained within a root-mean-square deviation (RMSD) of 0.18 Å from the initial coordinates.

The main characteristics of Pkn A and B consist of a transmembrane receptor with a tyrosine kinase domain protruding into the cytoplasm. For Pkn G, the unique multidomain topology of this PK reveals a central kinase domain that is flanked by N- and C-terminal rubredoxin and tetratrico-peptide repeat domains, respectively[13, 14].

The molecular datasets used for the docking study were reported by Sipos et al.[4], Székely et al.[5], Lougheed et al.[6], Chapman et al.[7] and finally Pato et al.[8] (see Table 1–Table 6). To select this molecular dataset, the structural diversity and uniform distribution of IC_{50} was taken into account. Logarithmic IC_{50} (μM) ($pIC_{50}=-\log IC_{50}$) was employed as the dependent variable instead of IC_{50}. The 3D molecular structures of the compounds were drawn and optimized using Maestro[15] and then prepared with the LigPrep module[16], where ionization/tautomeric states were predicted at physiological pH conditions

Table 1. Structures and pIC$_{50}$ values of the Pkn A ligands.

Compound[a]	Structure	pIC$_{50}$
1		-1.568
2		-1.839
3		-1.875
4		-1.934

[a]Compounds to Pkn A reported by Sipos et al.[4]

Table 2. Structures and pIC$_{50}$ values of the Pkn B ligands.

Compound	Structure	pIC$_{50}$
5[a,b]		-0.585 Pkn G:1.301
6[a]		0.569
7[a]		0.086
8[a]		0.585
9[a]		0.237
10[c]		-0.375

Compound	Structure	pIC$_{50}$
11[d]		1.276
12[d]		1.252
13[d]		1.046
14[d]		0.285
15[d]		-1.219

Compound	Structure	pIC$_{50}$
16[d]		-0.1758
17[d]		0.462
18[d]		1.259
19[d]		1.017
20[d]		1.036
21[d]		-0.792
22[d]		1.187

[a]Compounds to Pkn A reported by Sipos et al.[4]

[b]This compound has biological activity to Pkn B and G. Sipos et al.[4]

[c]Compound to Pkn B reported by Székely et al.[5]

[d]Compound to Pkn B reported by Loughheed et al.[6]

Table 3. Structures and pIC$_{50}$ values of the Pkn B ligands.

Compound[a]	R^1	NHR^2	pIC$_{50}$
23			0.492
24	--H		0.344
25	--CH$_3$		-0.065
26			0.652
27			0.357
28			0.971
29			0,369
30		-	0.426
31		-	0,416
32		-	0.406
33		-	1.066
34		-	0.618
35		-	1.060
36		-	0.695
37		-	1.076

38		-	0.451
39		-	0.146
40		-	1.130
41		-	1.194
42		-	0.664
43		-	0.939

[a]Compounds to Pkn B reported by Chapman *et al.*[7]

Table 4. Structures and pIC$_{50}$ values of the Pkn B ligands.

(compounds 44-49)

(compounds 50-53)

Compound[a]	NR^{1}R^2 or OR^1	R^3	pIC$_{50}$
44		-	1.056
45		-	0.917
46		-	1.260
47		-	1.137
48		-	1.276
49		-	1.252
50		CN	1.252
51		CN	1.409
52		CN	1.638
53		SO$_2$Me	1.398

[a]Compounds to Pkn B reported by Chapman *et al.*[7]

Table 5. Structures and pIC$_{50}$ values of the Pkn B ligands.

Compound[a]	R^1	R^2	pIC$_{50}$
54	H	CN	-0.299
55	OMe	H	-0.053
56	Cl	H	0.754
57	CF$_3$	CN	1.398

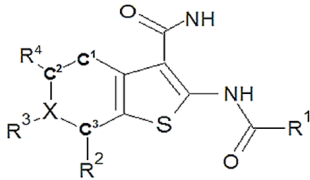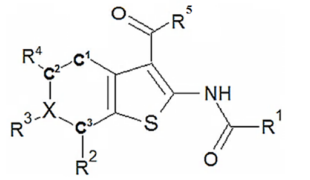[a]Compounds to Pkn B reported by Chapman *et al.*[7]

using Epik[17]. Afterwards, energy minimization was performed using Macromodel[18] with the OPLS2005 force field. The open-source software AutoDock Vina could also be used to perform these steps.

Docking studies were performed with the software Glide[18] using standard precision (SP) mode and default parameters. The open-source software AutoDock Vina could also be used to obtain similar results. The docking grid was generated with standard protocol centered at the co-crystallized ligand. Due to that, the scaling factor for the van der Waals interactions is very important it was taken as 0.8. The radii of nonpolar protein atoms were selected to allow the binding of larger ligands. Further, the induced fit docking (IFD) workflow[19] was also used to generate a good number of conformations of the receptor suitable for binding ligands that had strange orientations. It allows the protein to undergo side-chain movements, backbone movements, or both, upon ligand docking. The docking procedure has four steps where accuracy is ensured by Glide's scoring function and Prime's:

(i) The first step for Glide docking is carry out into the rigid receptor to generate a good ensemble of poses.

(ii) Analysis of the protein using Prime[21]. Taking into account side-chain prediction module followed by a structure energy minimization of each protein/ligand complex pose.

(iii) Analysis through re-docking of the ligand into low energy induced-fit structures taking in account the previous step using default Glide settings (no vdW scaling).

(iv) Finally, the binding energy is estimated using (IFDScore) by accounting for the docking energy (GScore), as well as receptor strain and some solvation terms (Prime energy).

To obtain the docking outcomes, the dynamics simulation of 100ns in vacuo using the GROMOS11 force field set was used

Table 6. Structures and pIC$_{50}$ values of the Pkn G ligands.

	(Compounds 58-72)					(Compounds 73,74)			

C	R^1	R^2	R^3	R^4	R^5	X	Bond C^3-X	Bond C^1-C^2	pIC$_{50}$
58[a]	cyclopropyl	H	H	H	NH	C	C^3-X	C^1-C^2	0.523
59[a]	cyclohexyl	H	-	H	NH	O	C^3-X	C^1-C^2	0.167
60[a]	cyclopropyl	H	-	H	NH	O	C^3-X	C^1-C^2	0.276
61[a]	isopropyl	H	-OH	H	NH	C	C^3=X	C^1=C^2	1.523
62[a]	cyclopropyl	Br	-OH	H	NH	C	C^3=X	C^1=C^2	1.699
63[a]	methy-cyclopropyl	Cl	-OH	H	NH	C	C^3=X	C^1=C^2	1.699
64[a]	methy-cyclopropyl	Cl	-OH	H	NH	C	C^3=X	C^1=C^2	1.699
65[a]	cyclopropyl	Cl	-OCH$_3$	Cl	NH	C	C^3=X	C^1=C^2	1.398
66[a]	1,3-benzodioxole	Cl	-OH	H	NH	C	C^3=X	C^1=C^2	2.000
67[a]	methy-cyclopropyl	H	-OH	H	NH	C	C^3=X	C^1=C^2	1.301
68[a]	methy-cyclopropyl	H	-OH	H	NH	C	C^3=X	C^1=C^2	1.301
69[b]	p-methylbenzoate	H	H	H	NH	C	C^3-X	C^1-C^2	0.699
70[b]	isopropyl	H	H	H	NH	C	C^3-X	C^1-C^2	-0.478
71[b]	Cyclobutyl	H	H	H	NH	C	C^3-X	C^1-C^2	-0.477
72[b]	methyl-isopropyl	H	H	H	NH	C	C^3-X	C^1-C^2	-1.176
73[b]	cyclopropyl	H	-Me	H	NH	C	C^3-X	C^1-C^2	0.046
74[b]	-Me	H	-Me	H	NH	C	C^3-X	C^1-C^2	-1.079
75[b]	cyclopropyl	H	H	H	NH	S	C^3-X	C^1-C^2	-0.301
76[b]	Furanyl	H	H	H	C$_2$H$_4$OH	C	C^3-X	C^1-C^2	-1.204
77[b]	cyclopropyl	H	H	H	OH	C	C^3-X	C^1-C^2	-1.279

[a]Compounds to Pkn G reported by Sipos et al.[4]

[b]Compounds to Pkn G reported by Pato et al.[8]

on the protein–ligand complex, using Gromacs 5.1.2[20] to analyze the stability of the protein–ligand complexes[22].

MQS analysis

In recent studies, MQS methodology has shown good results in understanding steric and electronic effects of ligands[23,24]. The MQS field was introduced by Carbó and co-workers 30 years ago[25–30] and has been used to understand the steric and electronic effect on the molecular sets. The mathematic relationship to obtain quantum similarity Z_{AB} between two compounds A and B, with electron density $\rho_A(r_1)$ and $\rho_B(r_2)$ is defined using

the minimization of the expression for the Euclidean distance as:

$$D_{AB} = \left(\int |\rho_A(r) - \rho_B(r)|^2 dr \right)^{1/2}$$
$$= \left(\int (\rho_A(r_1))^2 dr_1 + \int (\rho_B(r_2))^2 dr_2 - 2\int \rho_A(r_1)\rho_B(r_2) dr_1 dr_2 \right)^{1/2} \quad (1)$$
$$= (Z_{AA} + Z_{BB} - 2Z_{AB})^{1/2}$$

Therefore, the Euclidean distance is the square root of the integral on the squared differences between the densities $\rho_A(r_1)$ and $\rho_B(r_2)$. In this context, Z_{AB} represents the similarity measure

between the electronic densities of the compounds A and B, and Z_{AA} and Z_{BB} are the self-similarity of compounds A and B[31]. The similarity index very often used is the Carbó index[31]. This index is expressed as follows:

$$I_{AB} = \frac{\int \rho_A(r_1)\rho_B(r_2)dr_1dr_2}{\left(\int (\rho_A(r_1))^2 dr_1 \int (\rho_B(r_2))^2 dr_2\right)^{1/2}} = \frac{Z_{AB}(\mathbf{\Omega})}{(Z_{AA}(\mathbf{\Omega})Z_{BB}(\mathbf{\Omega}))^{1/2}} \quad (2)$$

In Equation 2, (Ω) represents an operator. A simple way to make quantum similarity measures (QSM)[29–31] involving two density functions, in the most usual form, is expressed as an integral:

$$Z_{AB}(\Omega) = \iint \rho_A(r_1)\Omega(r_1,r_2)\rho_B(r_2)dr_1dr_2 \quad (3)$$

In this equation $\rho_A(r_1)$ and $\rho_B(r_2)$ are the density functions to quantum objects A and B, while $\mathbf{\Omega}(r_1,r_2)$ is a positive operator that defines weight. The Dirac delta function: $\delta(r_1 - r_2)$ is used to obtain the overlap similarity measure and to measure the Coulomb similarity the Coulomb operator: $|r_1 - r_2|^{-1}$ is used. These operators are the most useful for obtaining similarity comparisons between ligands.

Molecular alignment
An important factor when carrying out the QSM is an optimal molecular alignment. As the integrals associated to the QSM produce, in any case, real positive results, the relative position problem can be approached using a maximal QSM. An overlap QSM can be expressed according to the equation:

$$\max_{T;\phi} Z_{AB}(T;\phi) = \max_{T;\phi} \int \rho_A(r)\rho_B(r|T;\phi)dr \quad (4)$$

In this equation, it is implicitly supposed that $\rho_B(r)$ is translated and rotated by the six possible ways: (T;φ) and are shown as explicit parameters in this integral[31]. This key factor was applied using the topo geometrical superposition algorithm (TGSA)[31].

Density functional theory (DFT) calculations
The calculations of this study were performed with the GAUSSIAN 09 program[32]. The open-source software AutoDock Vina could also be used to obtain similar results. The structures were optimized using the B3LYP functional (DFT exchange-correlation method)[33,34] and the 6-31G(d,p) basis set[35]. The contour lines of the molecular electrostatic potential have been obtained with the GaussView program[36].

Results and discussion
Pkn A, B and G: docking of their ATP-competitive inhibitors
The conformational analysis of the STPKs defines the active and inactive form. These forms are also known as the DFG-in and DFG-out states. They are distinguishable by a flip of the Asp and Phe orientation in the activation loop as well as conformational changes in the surrounding loops[37]. The main difference between DFG-in and DFG-out conformations is that the different position of the DFG residue in the "out" form results in the opening of an additional cavity, the allosteric site, which

can be hydrophobic in nature according to Zuccotto et al.[38]. In Pkn A the Asp side chain is buried and the Phe side chain is flipped outside the pocket. Therefore, Pkn A becomes DFG-out. However, in the STPKs Pkn B1 (crystal: 1MRU), Pkn B2 (crystal: 2FUM) and Pkn B3 (crystal: 3F69), the Asp side chain is exposed and the Phe side chain is buried (DFG-in), allowing ATP binding. Pkn G has DLG (Asp-Leu-Gly) instead of DFG (see Figure 1); the conformation is DLG-in. An important residue of STPKs is the gatekeeper. Their size determines the access of small, medium and large inhibitors to the back cavity even from the DFG-in state. In these crystallized PKs, the gatekeeper residues are MET95 for Pkn A, MET92 for Pkn B1 (crystal: 3F69), Pkn B2 (crystal: 1MRU), Pkn B3 (crystal: 2FUM), and MET232 for Pkn G. The methionine is a medium gatekeeper residue, according to Zuccotto et al.[38] and allows access to small, medium and large inhibitors. This characteristic is important because it increases the range of molecular diversity in the development of new inhibitors.

In Figure 1D, 1E and 1F we can see the hydrogen-bond-acceptor maps in red mesh. Pkn A shows a small red contour on the hinge zone (Figure 1D), a medium contour near to the DFG motif and a large contour near to the helix-αC and C-terminal loop. This is unlike Pkn B, which, using the crystal 3F69 (Figure 1E), shows only acceptor maps near to the DFG motif and in the C-terminal loop. Pkn G (Figure 1F) has large acceptor contours involving the hinge zone, DLG zone, helix-αC and C-terminal loop. Figure 1G, 1H and 1I shows the hydrogen-bond donor maps in blue mesh. In Pkn A (Figure 1G) we can see medium contours to hydrogen-bond donor on the hinge zone and C-terminal loop and a large contour near the DFG motif. In contrast, Pkn B (Figure 1H) shows only a large contour near to the DFG motif. Pkn G (Figure 1I) has small contours to hydrogen-bond donors along the hinge zone and near the DLG motif, helix-αC, C-terminal and N-terminal loops.

Analyses of hydrophobicity are shown in Figure 1J, 1K and 1L. Figure 1J shows a large contour of hydrophobicity for Pkn A near to the hinge zone and small contours on the C-terminal loop. Pkn B (Figure 1K) has only a small contour on the C-terminal loop. In contrast, Pkn G (Figure 1J) shows a large contour near the hinge zone, DLG motif and small contours near to the helix-αC and C-terminal loop. These physical-chemistry properties are important to describe the non-covalent stabilization on the active sites and selectivity of the ligands in the active pocket.

Pkn A: Descriptions of the structural characteristics of ATP binding sites and docking of inhibitors
To obtain the docking outcomes, hydrogen bonds on the hinge zone and non-covalent interactions near the "gatekeeper door", helix-αC, C-terminal and N-terminal were analyzed. An important insight are the non-covalent interactions. Theses interactions involved backbone, side chain hydrogen bonds and aromatic-aromatic interactions. On the other hand, the ligands with high scores have these characteristics in their non-covalent interactions. The ligands with lower scores have few to no interaction
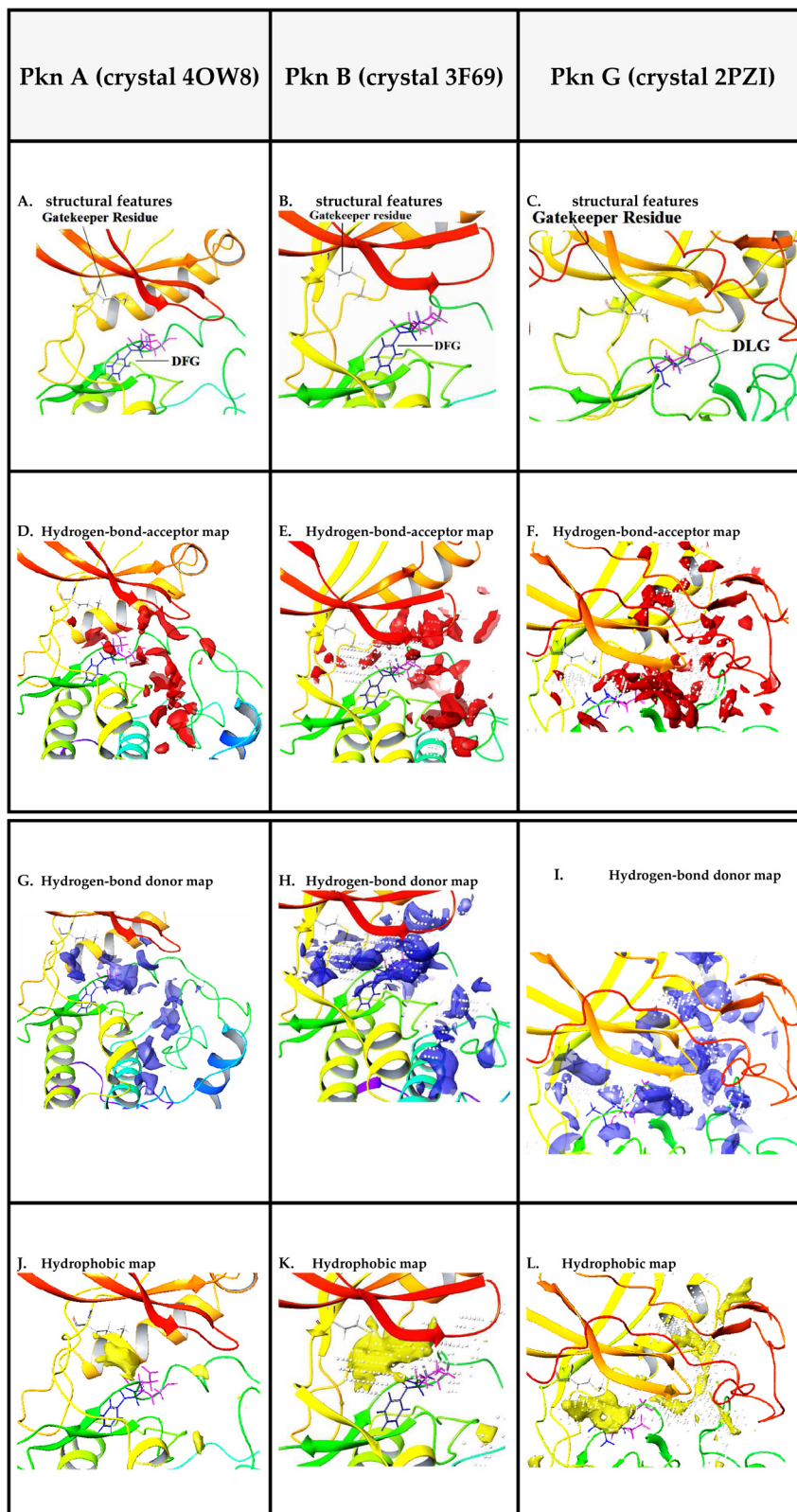
Figure 1. DFG conformational analysis and gatekeeper residues to STPKs crystalized from *Mycobacterium tuberculosis* for (**A**) Pkn A, (**B**) Pkn B and (**C**) Pkn G. Hydrogen-bond-acceptor map (red mesh) for (**D**) Pkn A, (**E**) Pkn B and (**F**) Pkn G. Hydrogen-bond donor map (blue mesh) for (**G**) Pkn A, (**H**) Pkn B and (**I**) Pkn G. Hydrophobic map for (**J**) Pkn, (**K**) Pkn B and (**L**) Pkn G. Note: map sites were calculated using SiteMAP in Maestro. The open-source software AutoDock Vina could also be used to obtain similar results.

forces. Further, some of the higher scoring ligands forming hydrogen bonds and aromatic-aromatic interactions with the amino acid residues are related to the hinge zone.

Figure 2 shows the docking interactions of the Pkn A inhibitors from Table 1. These compounds have groups with electron withdrawing resonance effects such as nitro, amine, carbonyl groups and electron donating groups such as methylene.

In Figure 2A we can see the hydrogen bonds on the hinge zone to compound 1 (Table 1). This compound has two interactions on the hinge zone with the residues Glu96, Val98 of 2.29 Å and 2.54 Å, respectively. Another hydrogen bond can be formed with the residue Asn104 of 1.98 Å. Compounds 2, 3 and 4, see Figure 2B, have differences only in the substituent group, in the case of 3, this is a pyrrole ring and in 4, is the dimethylamine group. In this series, the most active compound is 2, with pIC_{50} -1.839. These compounds show two hydrogen bonds on the hinge zone with residues Glu96 and Val98 of 1.31 Å and 2.30 Å to 2, 1.71 Å and 2.35 Å to 3 and 1.81 Å and 2.21 Å

to 4. Another hydrogen bond can also be formed with the residue Gly145 of 2.22 Å to 2, 1.81 Å to 3 and 1.95 Å to 4. From these results, we can see the key factor to the stabilization of the active site in this ligand set, with the main characteristic of one H-bond acceptor and H-bond donor in this zone.

Figure 3 (left) and Figure 4 show, respectively, the atomic charges calculated by the CHelpG population and electrostatic potential analyses of compound 1 in some areas of special interest. The net charges obtained for H22, O24, O30 and O31 are consistent with the formation of hydrogen bonds shown in Figure 2A. The electrostatic potential surfaces shown in Figure 4 also justify the formation of hydrogen bonds with Glu96, Val98 and Asn104. Figure 3 (right) and Figure 5 show, respectively, the atomic charges and electrostatic potential of compound 4. The atomic charges of H27, H42 and H15 justify very well the formation of hydrogen bonds with Glu96, Val98 and Asn104 that can be seen in Figure 2B. An equivalent conclusion can be found from the electrostatic potential surfaces shown in Figure 5.
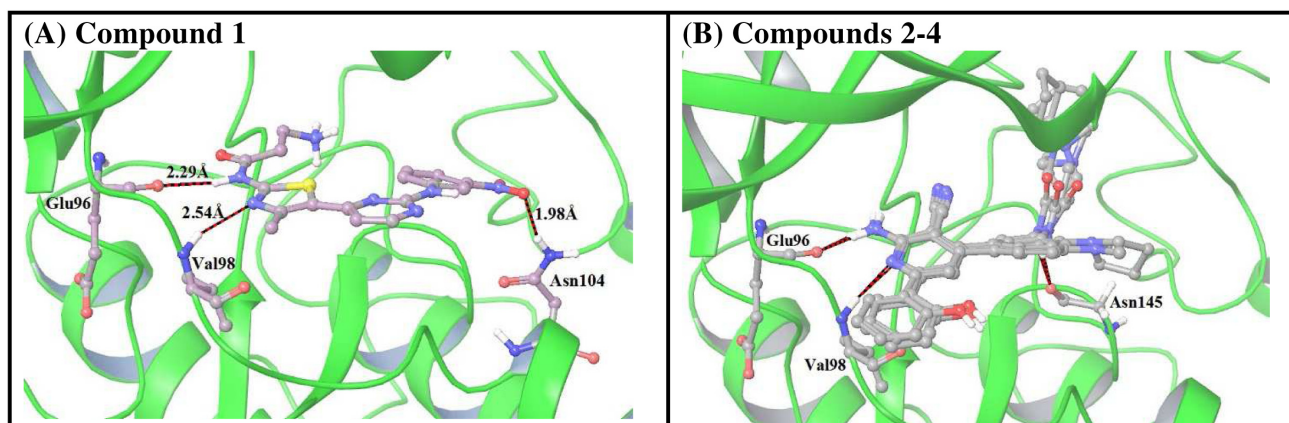

Figure 2. Interactions on the hinge zone of compound 1 (**A**) and compounds 2-4 aligned (**B**), from Table 1.
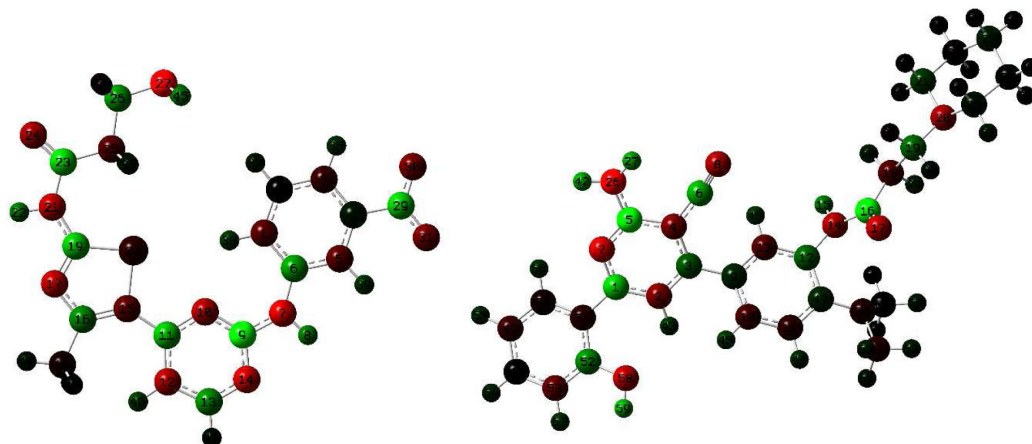

Figure 3. CHelpG charges calculated for compounds 1 (left) and 4 (right).
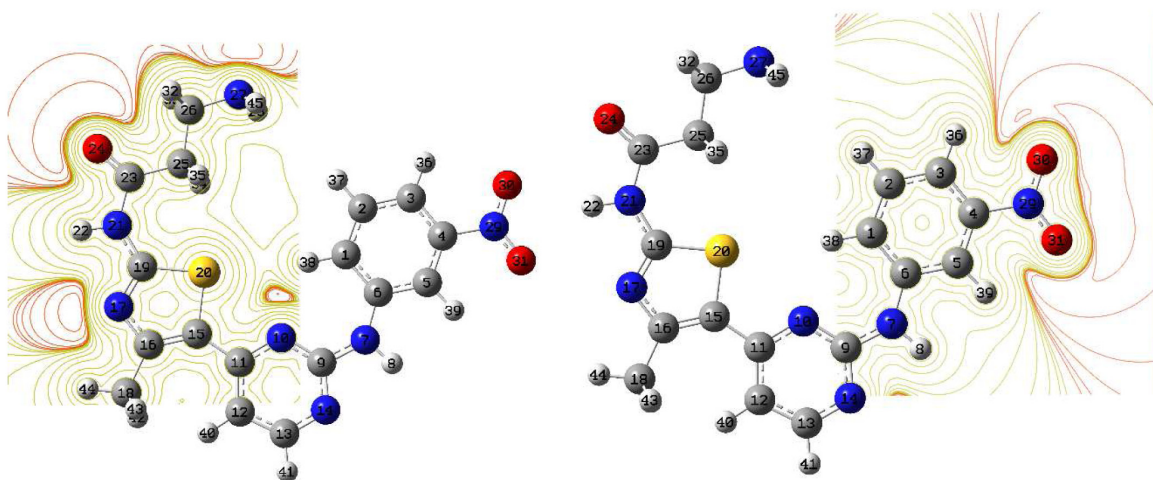
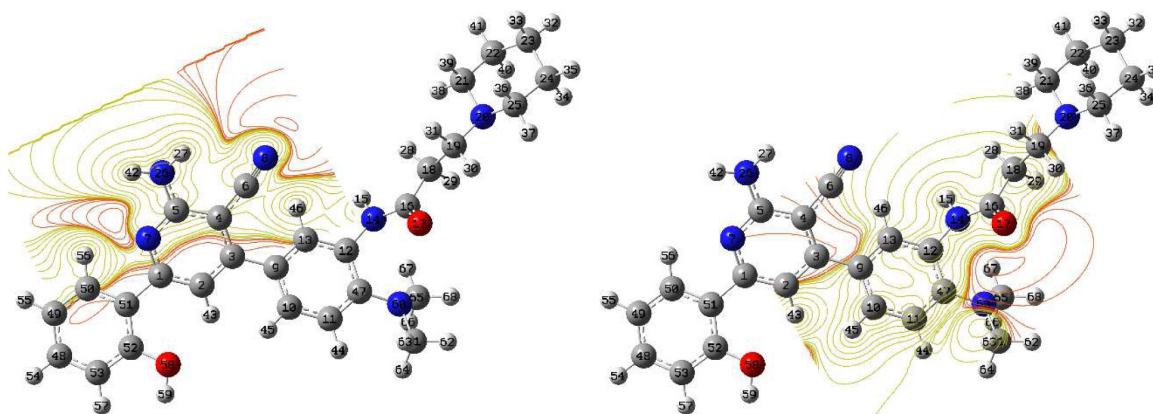**Figure 4. Molecular electrostatic potential contour lines of compound 1.**

Figure 5. Molecular electrostatic potential contour lines of compound 4.

Pkn B: Descriptions of the structural characteristics of ATP binding sites and docking of inhibitors

The compounds to Pkn B have groups with electron withdrawing resonance effects, such as carbonyl, hydroxyl, amine and methoxy groups, with big rings central to its stabilization on the active site. Figure 6 shows the docking results of the Pkn B inhibitors from Table 2–Table 5, grouped by series, taking into account their functional groups and structural similarities. Figure 6A shows compound 5, which has interactions in the hinge zone with the residues Glu93 (2.63Å) and Val95 (-CO: 2.46Å, -NH: 1.99Å, 2.16Å), see Table 7. Compound 5 has dual effects, interacting with Pkn B (pIC$_{50}$: -0.585) and Pkn G (pIC$_{50}$: 1.301), see Table 2. Figure 6B shows the interaction with compound 6, which has interactions with the residue Val95 (-CO: 1.31Å, -NH: 2.48Å). In these interactions the -NH is H-bond donor and the –CO is H-bond acceptor; these interactions can be related to the pIC$_{50}$ of 0.569 for this compound.

Figure 6C shows the interaction in the hinge zone to of compounds 7, 8 and 9. These compounds have two interactions in the hinge zone with the residue Val95. The most active compound of this series is 8 (pIC$_{50}$: 0.585) with its interactions with the residue Val95 (-CO: 1.80Å, -NH: 2.15Å), see Table 7. Figure 6D shows the interactions of the compound 10; this compound has two interactions in the hinge zone with the residue Val95 (-NH: 2.33Å, -C=O: 2.09Å). Another H-bond happens with the residues Asp96 (1.71Å) Asp102 (-C=O: 2.42Å, -OH: 2.10Å) and Lys140 (2.01Å). The interactions with the two guanidine groups are through the aspartates. This is very interesting because these kinds of interactions could differentiate one kinase from another. Figure 6E shows the interactions in the hinge zone of the compounds 11, 12, 17, 18, 19, 20 and 23–53. This series of compounds have three H-bonds in the hinge zone with the residues Glu93 and Val95. The most active compound from this series is 52 (pIC$_{50}$: 1.638). It has
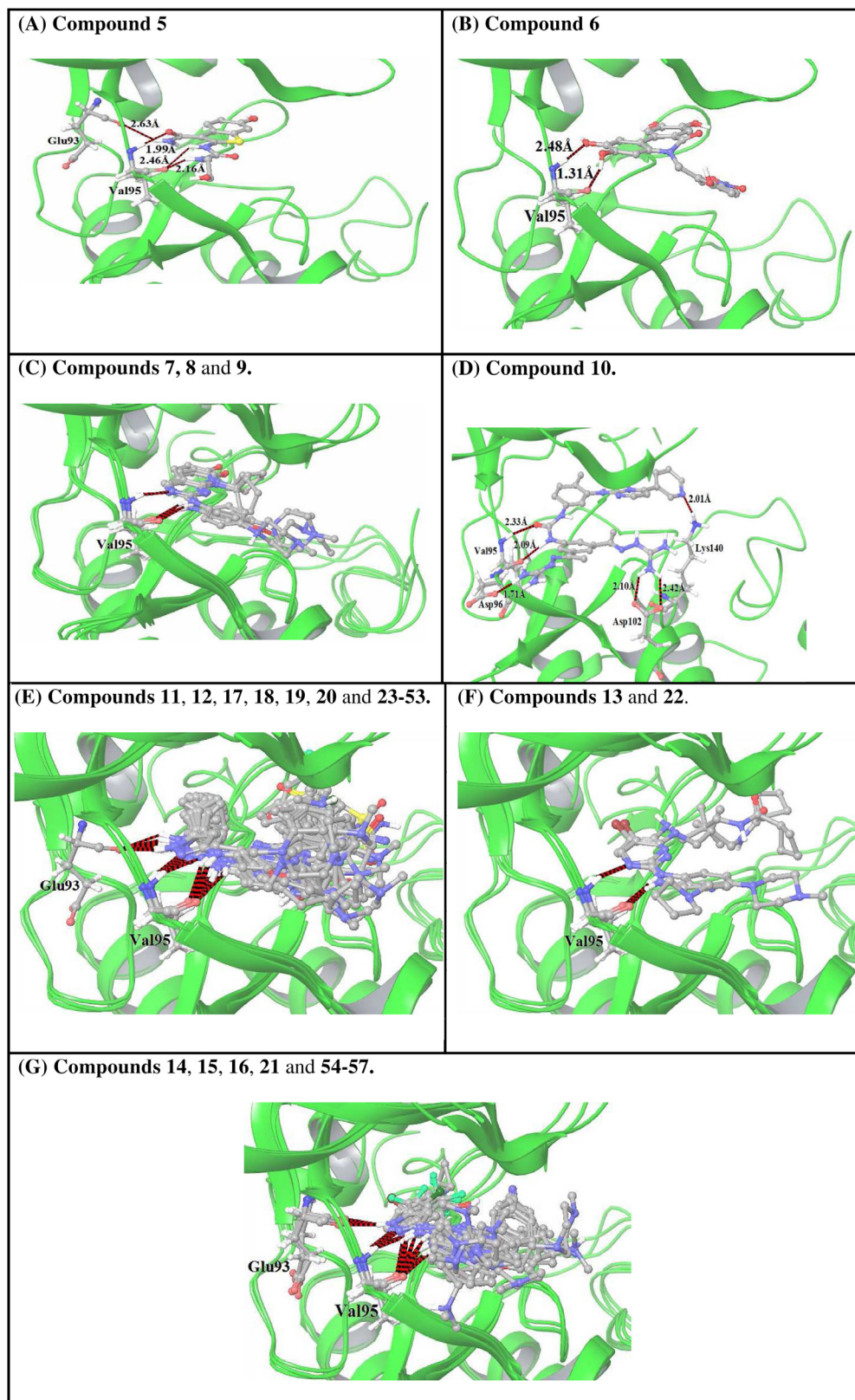
Figure 6. Interactions in the hinge zone with compound 5 (**A**); compound 6 (**B**); compounds 7, 8, 9 (**C**); compound 10 (**D**); compounds 11, 12, 17, 18, 19, 20 and 23-53 (**E**); compounds 13 and 22 (**F**); and compounds 14, 15, 16, 21 and 54-57 (**G**), from Table 2–Table 5.

Table 7. Hydrogen bonds in the hinge zone and other zones to the Pkn B inhibitors (Table 2), distance in Å.

Compound	Hinge zone			Others (–H bonds)	Crystal PDB ID
	Glu93	Val95 (-C=O)	Val95 (-NH)		
5	2.63	1.99	2.46, 2.16	Asp96:1.97	1MRU
6	-	1.31	2.48	Leu17:1.97 Lys401.75	1MRU
7	2.31	2.15	-	-	2FUM
8	2.15	1.80	-	-	2FUM
9	2.22	2.07	-	-	2FUM
10	2.33	2.09	-	Asp96:1.71 Lys140:2.01 Asp102:2.42 (-C=O), 2.10 (-OH)	3F69
11	1.94	2.51	2.16		3F69
12	2.42	2.34	2.42		3F69
13	-	2.39	2.42	-	3F69
14	-	2.40	2.45	-	3F69
15	-	1.98	2.40	Glu15:2.73	2FUM
16	-	2.08	2.25	-	2FUM
17	1.94	2.38	2.09	-	3F69
18	1.89	2.73	2.32	-	3F69
19	2.56	2.65	2.18	-	1MRU
20	2.46	2.19	2.02	-	1MRU
21	-	2.30	2.38	-	1MRU
22	-	2.27	1.90	Gly97:2.02	3F69
23	1.93	-	2.27	-	3F69
24	1.72	-	2.21	-	3F69
25	1.88	-	2.44	-	3F69
26	1.97	-	2.28	-	3F69
27	1.93	-	2.28	-	3F69
28	1.87	-	2.39	-	3F69
29	1.98	-	2.14	-	3F69
30	1.91	2.27	2.09	-	3F69
31	1.91	2.44	2.13	-	3F69
32	1.93	2.25	2.05	-	3F69
33	1.91	2.31	2.12	-	3F69
34	1.91	2.21	2.07	-	3F69
35	1.92	2.16	2.08	-	3F69
36	1.91	2.23	2.07	-	3F69

Compound	Hinge zone			Others (–H bonds)	Crystal PDB ID
	Glu93	Val95 (-C=O)	Val95 (-NH)		
37	1.91	2.24	2.08	-	3F69
38	1.94	2.10	2.10	-	3F69
39	1.91	2.20	2.07	-	3F69
40	1.91	2.21	2.08	-	3F69
41	2.19	2.05	2.20	-	3F69
42	1.99	1.96	2.06	-	3F69
43	1.92	2.16	2.09	-	3F69
44	1.96	2.14	2.13	Gly97:2.01	3F69
45	1.92	2.42	2.13	-	3F69
46	1.91	2.34	2.11	Gly97:2.19	3F69
47	1.93	2.35	2.19	Gly97:2.21	3F69
48	1.59	2.46	2.05	-	3F69
49	2.64	2.67	2.13	-	1MRU
50	2.07	2.26	1.80	-	1MRU
51	1.94	2.20	2.16	Gly97:2.04	1MRU
52	2.21	2.33	1.85	-	1MRU
53	2.27	2.19	2.27	-	3F69
54	-	2.72	2.44	-	1MRU
55	-	2.46	2.04	-	2FUM
56	-	2.23	2.12	-	1MRU
57	-	2.58	2.39	-	1MRU

interactions with residues Glu93 (2.21Å) and Val95 (-CO: 2.33Å, -NH: 1.85Å), see Table 7. In this series there are two –CO H bond acceptors and one -NH H bond acceptor. Figure 6F shows the interactions in the hinge zone of the compounds 13 and 22; these compounds have two interactions in the hinge zone with the residue Val95 (-CO: 2.39Å, -NH: 2.42Å for 13 and -CO: 2.27Å, -NH: 1.90Å for 22), see Table 7. The most active compound is 22 (pIC$_{50}$: 1.187). Finally, Figure 6G shows the interactions in the hinge zone of the compounds 14, 15, 16, 21 and 54–57. This series of compounds also has three interactions in the hinge zone with the residues Glu93 and Val95. The most active compound in this series is 57 (pIC$_{50}$: 1.398), see Table 5.

Taking in account the results from Table 7, the key factor to the stabilization of the active site of these ligands is one or two –CO (H bond acceptor) and one -NH (H bond acceptor) groups in this zone.

Figure 7 shows the atomic charges calculated with the CHelpG population analysis (upper left) and the electrostatic potential

(upper right and down) of compound 5 in some areas of special interest. The net charges obtained for H11, O13, H21 and H22 are consistent with the formation of hydrogen bonds shown in Figure 6A. The electrostatic potential of surfaces shown in Figure 7 also justify the formation of hydrogen bonds with Glu93 and Val95.

Figure 8 shows the atomic charges calculated by CHelpG population analysis (left) and the electrostatic potential (right) of compound 6 in some areas of special interest. The net charges obtained for H40 and O41 are consistent with the formation of hydrogen bonds shown in Figure 6B. The electrostatic potential of surfaces shown in Figure 8 also justify the formation of hydrogen bonds with Val95.

Figure 9 shows the atomic charges calculated by CHelpG population analysis (left) and the electrostatic potential (right) of compound 8 in some areas of special interest. The net charges obtained for N9 and H13 are consistent with the formation of hydrogen bonds shown in Figure 6C. The
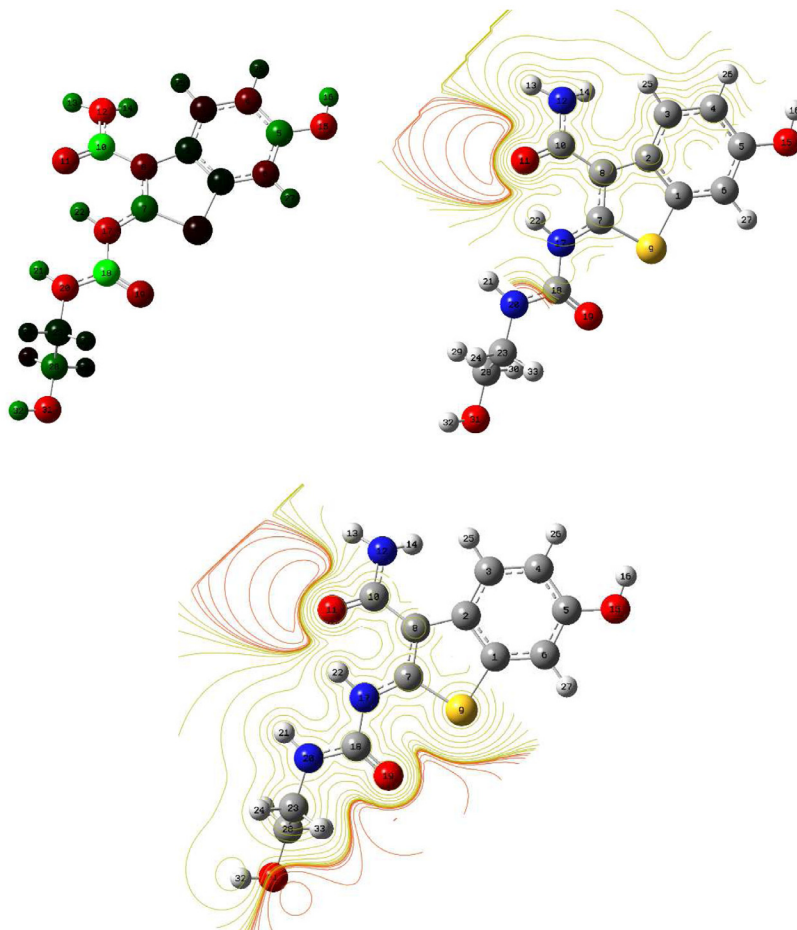
Figure 7. CHelpG charges (left) and molecular electrostatic potential contour lines (right and down) of compound 5.
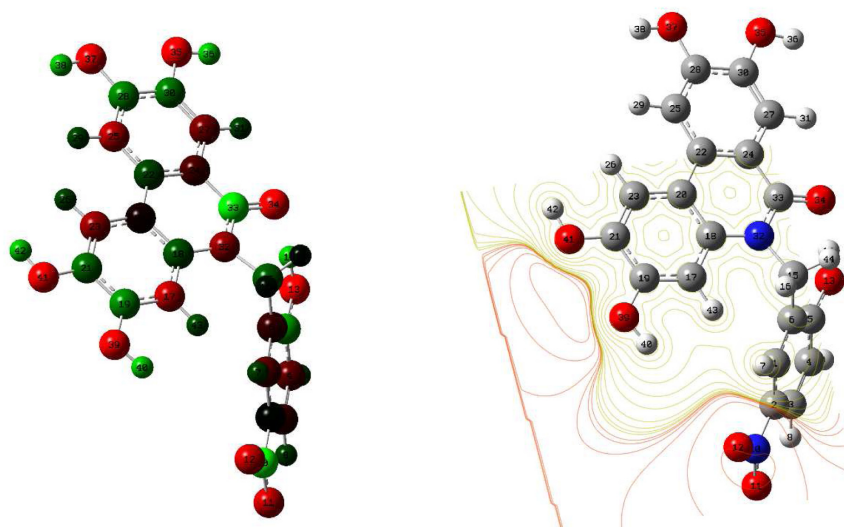

Figure 8. CHelpG Charges (left) and molecular electrostatic potential contour lines (right) of compound 6.

electrostatic potential of surfaces shown in Figure 9 also justify the formation of hydrogen bonds with Val95.

Figure 10 shows the atomic charges calculated by CHelpG population analysis (left) and the electrostatic potential (upper
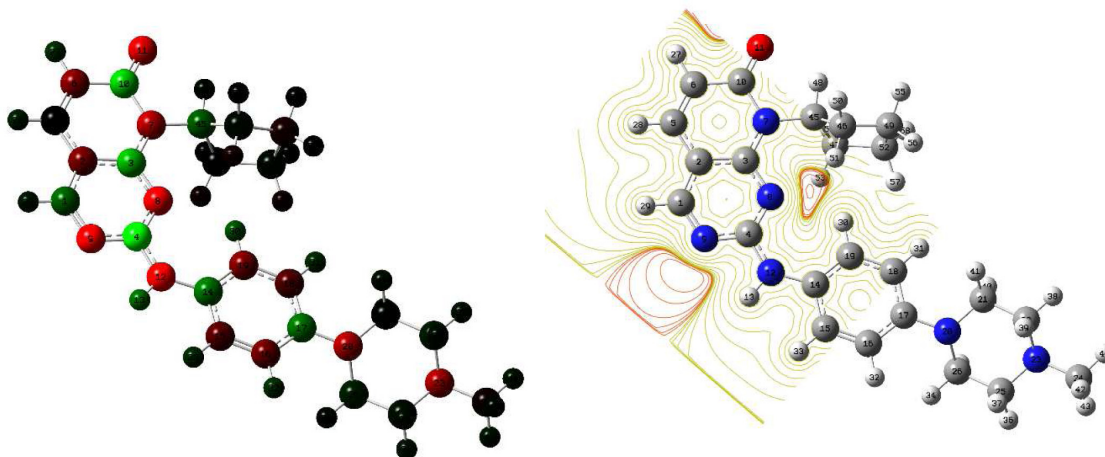

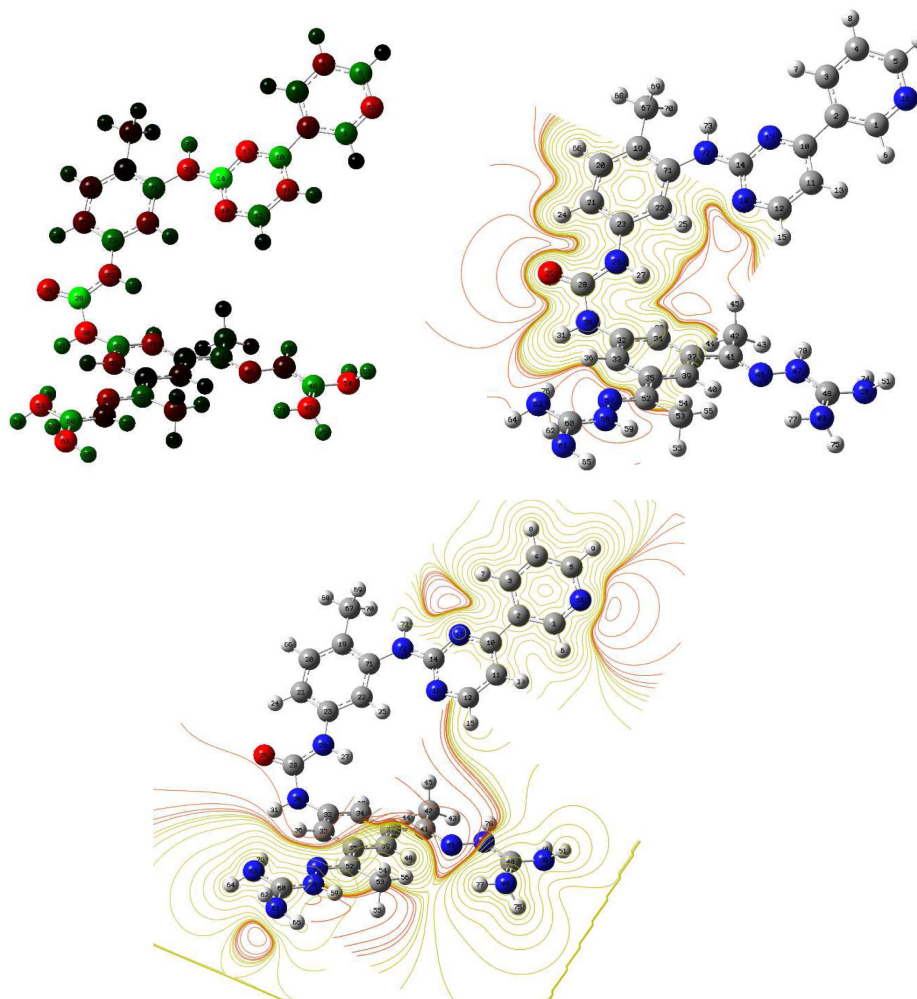**Figure 9. CHelpG charges (left) and molecular electrostatic potential contour lines (right) of compound 8.**

Figure 10. CHelpG charges (left) and molecular electrostatic potential contour lines (right and down) of compound 10.

right and lower) of compound 10 in some areas of special interest. The net charges obtained for O29, N31, N16, H64 and H76 are consistent with the formation of hydrogen bonds shown in Figure 6D. The electrostatic potential of surfaces shown in Figure 10 also justify the formation of hydrogen bonds with Val95 (O29 and N31), Lys140 (N16) and Asp102 (H64 and H76).

Figure 11 shows the electrostatic potential generated by compound 13 in some areas of special interest. The electrostatic potential of surfaces shown in Figure 11 are consistent with the

interactions shown in Figure 6F and justify the formation of hydrogen bonds of H34 and N36 with Val95.

Figure 12 shows the atomic charges calculated with the CHelpG population analysis (left) and the electrostatic potential (right) of compound 15. The net charges obtained for H31, H38 and N39 are consistent with the formation of hydrogen bonds shown in Figure 3G. The electrostatic potential of surfaces shown in Figure 12 also justify the formation of hydrogen bonds with Glu93 (H38) and Val95 (H31 and N39).
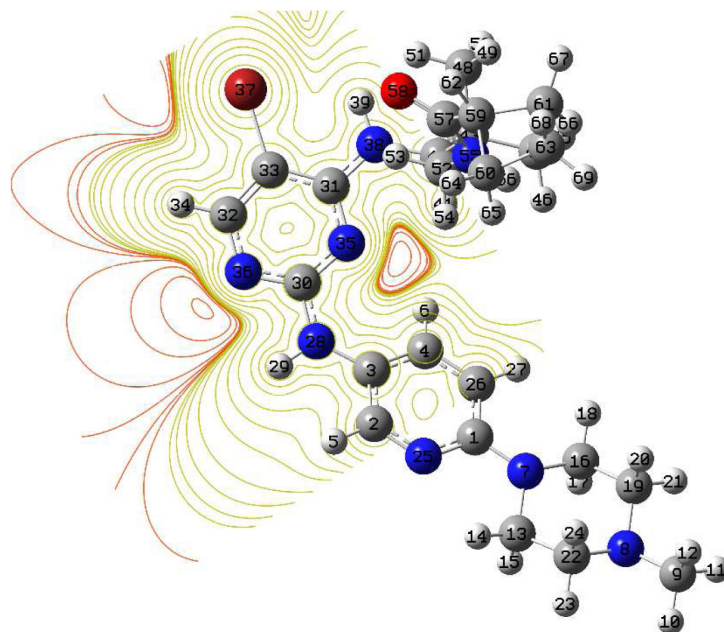

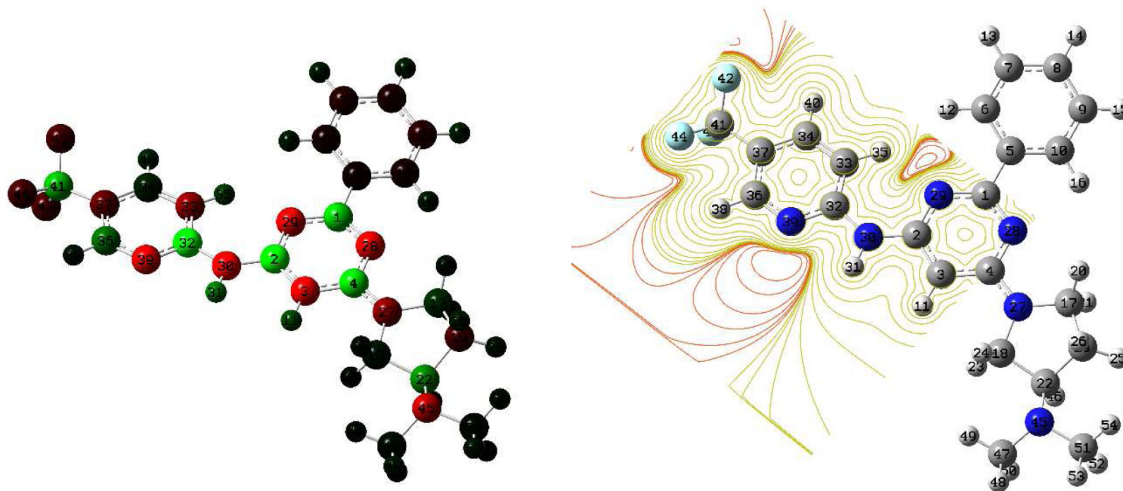**Figure 11. Molecular electrostatic potential contour lines of compound 13.**

Figure 12. CHelpG charges (left) and molecular electrostatic potential contour lines (right) of compound 15.

Pkn G: Descriptions of the structural characteristics of ATP binding sites and docking of inhibitors

The Pkn G inhibitors from Table 6 have a common structure and three interactions in the hinge zone with the residues Glu233 and Val 235 (see Figure 13).

The most active compound of this series is 66 (pIC_{50}: 2.000). This compound has interactions with the residue Glu93 (2.59Å) and Val95 (-CO: 2.24Å, -NH: 2.17Å), see Table 8. Other compounds with good reactivity are 62, 63C1 and 63C2 (pIC_{50}: 1.699). These compounds have interactions with the residues Glu93 (2.18Å), Val95 (-CO: 2.56Å, -NH:1.78 Å); Glu93 (2.36Å), Val95 (-CO: 2.18Å, -NH:1.90 Å) and Glu93 (2.10Å), Val95 (-CO: 2.22Å, -NH:1.89 Å), respectively. In these ligands the key factors are two –CO (H bond acceptor) and one -NH (H bond acceptor) groups for stabilizing the ATP active site.

Figure 14 shows the atomic charges calculated by CHelpG population analysis (left) and the electrostatic potential (right) of compound 58. The net charges obtained for H16, O11 and H14 are consistent with the formation of the hydrogen bonds
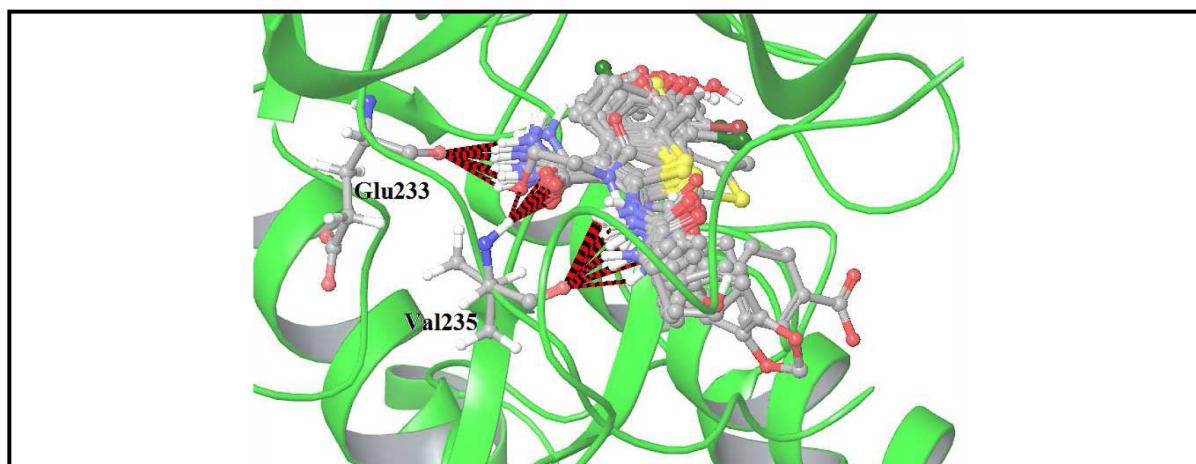

Figure 13. Interactions in the hinge zone of compounds 58-75 with Pkn G, from Table 6.

Table 8. Hydrogen bonds in the hinge zone and other zones with the Pkn G inhibitors (Table 6), distance in Å.

Compound	Hinge zone			Others (–H bonds)
	Glu233	Val235 (-C=O)	Val235 (-NH)	
58	1.99	2.37	1.80	-
59	2.27	2.74	2.36	-
60	2.07	2.51	1.88	-
61	2.57	2.57	2.18	-
62	2.18	2.56	1.78	-
63C1[a]	2.36	2.18	1.90	Lys181:2.33
64C2[a]	2.10	2.22	1.89	Asp293:1.68
65	2.69	2.64	1.93	Lys181:2.31
66	2.59	2.24	2.17	Lys181:2.16
67C1[a]	2.47	2.61	1.93	Asp293:2.00
68C2[a]	2.28	-	1.98	Asp293:1.81
69	2.43	2.67	1.87	-

Compound	Hinge zone			Others (–H bonds)
	Glu233	Val235 (-C=O)	Val235 (-NH)	
70	1.96	2.60	1.73	-
71	2.60	2.56	1.79	-
72	2.00	2.49	1.80	-
73	2.27	2.06	1.94	-
74	2.43	2.74	2.24	-
75	2.07	2.60	1.80	-
76	2.47	-	2.56	-
77	2.03	2.55	1.82	-

[a]Conformations with respect to the methyl in the cyclopropyl group.
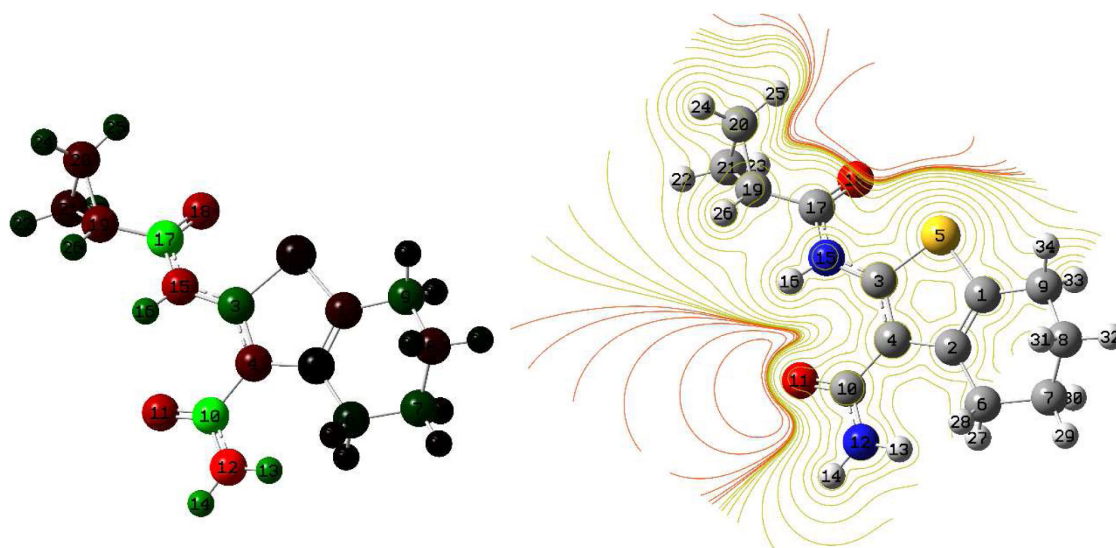

Figure 14. CHelpG charges (left) and molecular electrostatic potential contour lines (right) of compound 58.

shown in Figure 13. The electrostatic potential of surfaces shown in Figure 14 also justify the formation of hydrogen bonds with Glu233 (H16) and Val235 (O11 and H14).

MQS analysis

The MQS analysis was conducted to understand the correlation between the ATP ligands associated to each kinase studied and the stabilization process in the active site. This correlation allows postulation of the structural models of the ATP complexes.

For the Pkn A ligands (see Figure 15), the correlation between the steric and electronic effects is $R^2 = 0,9487$ using the coulomb and overlap operators to determine electronic and steric effects, respectively. This correlation shows the nature of

the stabilization of these ligands on the active site and its non-covalent character.

Figure 16 shows the correlation of Pkn B ligands (see Table 2–Table 5). This correlation shows the electronic and steric effects along the ligand set associated with the active site. The high values in the Carbó indexes give an idea about the ATP complex generated and stabilized.

In Figure 17 is shown the correlation between the steric and electronic effects associated with the ATP complex of Pkn G (see Table 6). This complex has a correlation of $R^2 = 0,7357$. In this complex, the steric and electronic effects also are very relevant and the stabilization in the active site has a high non-covalent character.
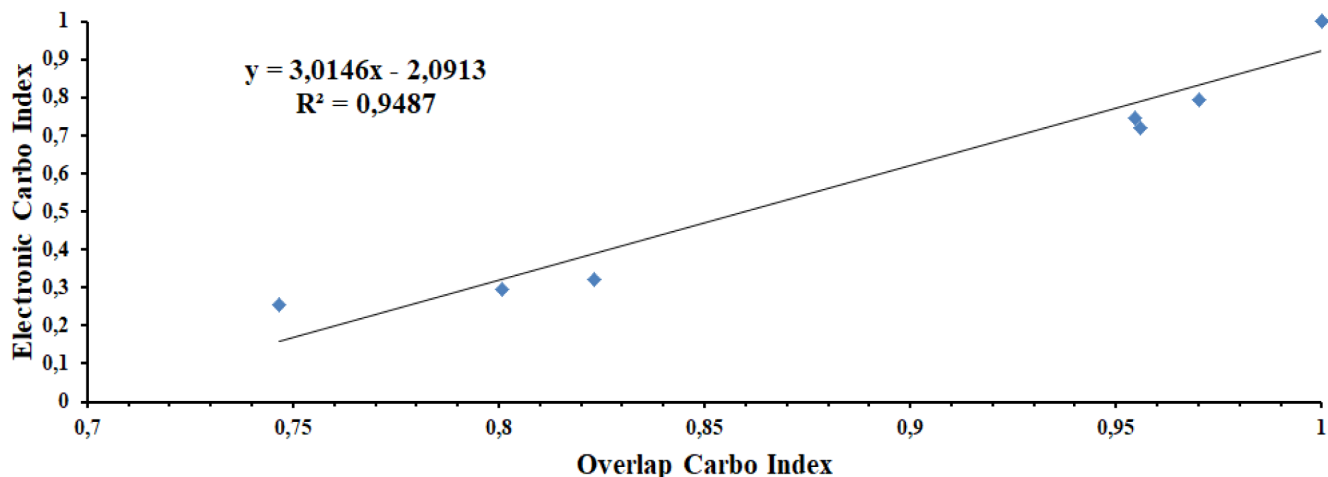
$$y = 3{,}0146x - 2{,}0913$$
$$R^2 = 0{,}9487$$

Figure 15. Electronic and steric effect correlation to Pkn A ligands.

$$y = 2{,}1902x - 1{,}3738$$
$$R^2 = 0{,}7515$$
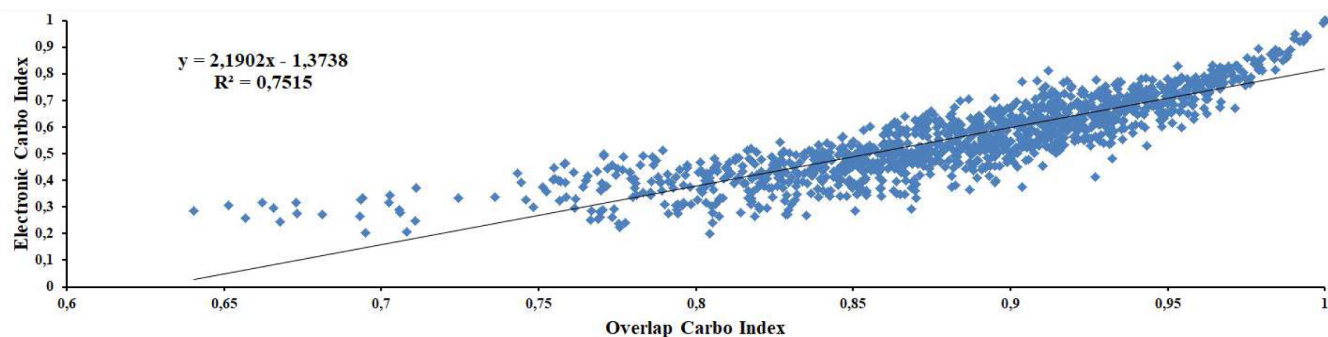
Figure 16. Electronic and steric effects correlation to Pkn B ligands.

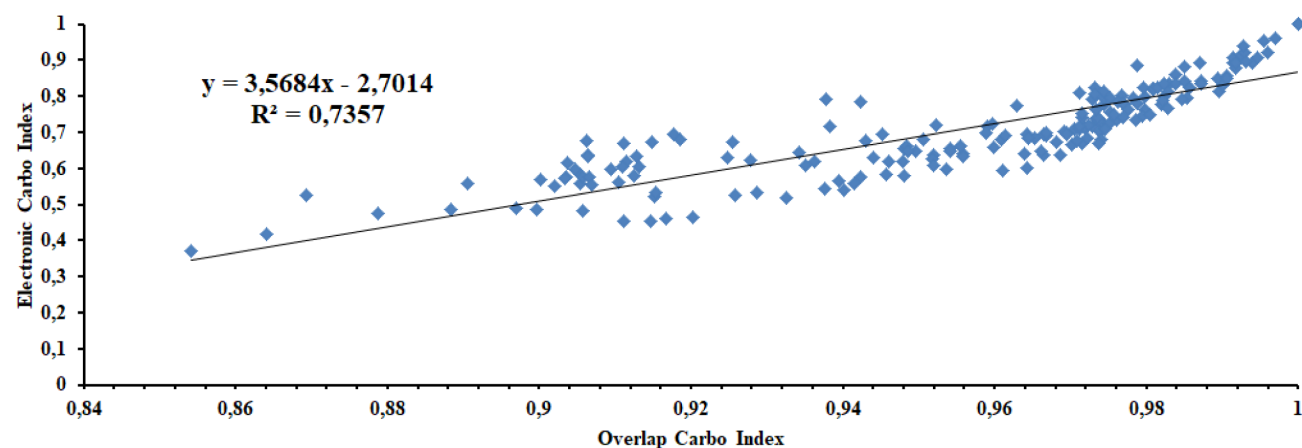$$y = 3{,}5684x - 2{,}7014$$
$$R^2 = 0{,}7357$$

Figure 17. Electronic and steric effects correlation to Pkn G ligands.

In Figure 15–Figure 17 a strong correlation between the two operators used to determine electronic and steric effects is shown. These effects can be related to the stabilization process and non-covalent interactions. In this way, the quantum

similarity analysis allows us study the ATP complex and understand the steric and electronic relationship along the ligand set.

Conclusions

Inadequate dosing and incomplete treatment regimens, coupled with the ability of the tuberculosis bacilli to cause latent infections that are tolerant of currently used drugs, have fueled the rise of multi-drug resistant tuberculosis. To deal with this problem, there is currently an increased interest in kinase inhibitors with the main aim of proposing new anti-tuberculosis drugs. For these reasons, in this work we conducted a study of the crystalized STPKs Pkn A, B1, B2, B3 and G. The conformational analysis shows the DFG-in state of Pkn B, G, and DFG-out state of Pkn A. Methionine is the gatekeeper residue in all the kinases studied.

To understand the interactions of the active site of the protein kinases from *Mycobacterium tuberculosis,* a docking study using the protein kinases Pkn A, B and G was conducted. In these protein kinases, the C-term domain is extracellular and N-term is cytosolic. The cytosolic domain is almost the same for all the kinases and the extracellular domain is different. Ligands bind to the kinase through the formation of two to three hydrogen bonds with the backbone residues of the hinge region connecting the kinase N- and C-terminal loops. The residues with hydrogen bonds on the hinge zone of Pkn A are GLU96 and VAL 98, of Pkn B are GLU 93 and VAL 95, and finally of Pkn G are GLU233 and VAL235. From these results, it is possible to see that the interactions of the hinge zone are characterized by the key factor of one or two H-bonds acceptors and one H-bond donor in the ligands of this zone. On the other hand, the DFT calculations performed with some of the most representative compounds have supported the previous conclusions. Finally, the quantum similarity analysis shows good correlation between the steric and electronic effects in each ATP complex. In this sense, the outcomes presented in this work can be used to develop new protein substrates of the STPKs and find new tuberculosis treatments.

Data availability

All data underlying the results are available as part of the article and no additional source data are required.

References

1. Hallows KR, Alzamora R, Li H: **AMP-activated protein kinase inhibits alkaline pH- and PKA-induced apical vacuolar H+-ATPase accumulation in epididymal clear cells.** *Am J Physiol Cell Physiol.* 2009; **296**(4): C672–81.
   PubMed Abstract | **Publisher Full Text** | **Free Full Text**

2. Av-Gay F, Everett M: **The eukaryotic-like Ser/Thr protein kinases of *Mycobacterium tuberculosis*.** *Trends in Microbiology.* 2000; **8**(5): 238–244.

3. Sipos A, Pató J, Székely R, *et al.*: **Lead selection and characterization of antitubercular compounds using the Nested Chemical Library.** *Tuberculosis (Edinb).* 2015; **95 Suppl 1**: S200–6.
   PubMed Abstract | **Publisher Full Text**

4. Székely R, Wáczek F, Szabadkai I, *et al.*: **A novel drug discovery concept for tuberculosis: inhibition of bacterial and host cell signalling.** *Immunol Lett.* 2008; **116**(2): 225–31.
   PubMed Abstract | **Publisher Full Text**

5. Lougheed KEA, Osborne SA, Saxty B, *et al.*: **Effective inhibitors of the essential kinase PknB and their potential as anti-mycobacterial agents.** *Tuberculosis (Edinb).* 2011; **91**(4): 277–86.
   PubMed Abstract | **Publisher Full Text** | **Free Full Text**

6. Chapman TM, Bouloc N, Buxton RS, *et al.*: **Substituted aminopyrimidine protein kinase B (PknB) inhibitors show activity against *Mycobacterium tuberculosis*.** *Bioorg Med Chem Lett.* 2012; **22**(9): 3349–53.
   PubMed Abstract | **Publisher Full Text** | **Free Full Text**

7. Pato J, Orfi L, Waczek F, *et al.*: **United States Patent Application Publication**. Pub: No.:US 2004/0171603 A1. 2004.

8. Ravala SK, Singh S, Yadav GS, *et al.*: **Evidence that phosphorylation of threonine in the GT motif triggers activation of PknA, a eukaryotic-type serine/threonine kinase from *Mycobacterium tuberculosis*.** *FEBS J.* 2015; **282**(8): 1419–31.
   PubMed Abstract | **Publisher Full Text**

9(a). (3f69) Mieczkowski C, Lavarone AT, Alber T: **Auto-activation mechanism of the *Mycobacterium tuberculosis* PknB receptor Ser/Thr kinase.** *Embo J.* 2008; **27**(23): 3186–3197.
   PubMed Abstract | **Publisher Full Text** | **Free Full Text**

(b). (2mru) Young TA, Delagoutte B, Endrizzi JA, *et al.*: **Structure of *Mycobacterium tuberculosis* PknB supports a universal activation mechanism for Ser/Thr protein kinases.** *Nat Struct Biol.* 2003; **10**(3): 168–74.
   PubMed Abstract | **Publisher Full Text**

(c). (2fum) Wehenkel A, Fernandez P, Bellinzoni M, *et al.*: **The structure of PknB in complex with mitoxantrone, an ATP-competitive inhibitor, suggests a mode of protein kinase regulation in mycobacteria.** *Embo J.* 2006; **580**(13): 3018–22.
   PubMed Abstract | **Publisher Full Text**

10. Scherr N, Honnappa S, Kunz G, *et al.*: **Structural basis for the specific inhibition of protein kinase G, a virulence factor of *Mycobacterium tuberculosis*.** *Proc Natl Acad Sci U S A.* 2007; **104**(29): 12151–6.
    PubMed Abstract | **Publisher Full Text** | **Free Full Text**

11. **Schrödinger Suite 2014-1 Protein Preparation Wizard; Epik version 2,7**. Schrödinger, LLC, New York, NY, 2013. Impact version 6,2, Schrödinger, LLC, New York, NY, 2014; Prime version 3,5, Schrödinger, LLC, New York, NY, 2014; (n,d,).

12. Olsson MHM, Søndergaard CR, Rostkowski M, *et al.*: **PROPKA3: Consistent Treatment of Internal and Surface Residues in Empirical pKa Predictions.** *J Chem Theo Comp.* 2011; **7**(2): 525–537.
    PubMed Abstract | **Publisher Full Text**

13. Banks JL, Beard HS, Cao Y, *et al.*: **Integrated Modeling Program, Applied Chemical Theory (IMPACT).** *J Comput Chem.* 2005; **26**(16): 1752–80.
    PubMed Abstract | **Publisher Full Text** | **Free Full Text**

14. Malhotra V, Arteaga-Cortés LT, Clay G, *et al.*: ***Mycobacterium tuberculosis* protein kinase K confers survival advantage during early infection in mice and regulates growth in culture and during persistent infection: implications for immune modulation.** *Microbiology (Reading).* 2010; **156**(Pt 9): 2829–2841.
    PubMed Abstract | **Publisher Full Text** | **Free Full Text**

15. **Maestro, version 9,7**. Schrödinger, LLC, New York, NY. 2014; (n,d,).

16. **LigPrep, version 2,9**. Schrödinger, LLC, New York, NY. 2014; (n,d,).

17. **Epik, version 2,7**. Schrödinger, LLC New York, NY. 2014; (n,d,).

18. **Schrödinger Suite 2014-2 Induced Fit Docking protocol; Glide, version 6.2**. Schrödinger, LLC, New York, NY. 2014.

19. Sherman W, Day T, Jacobson MP, *et al.*: **Novel procedure for modeling ligand/receptor induced fit effects.** *J Med Chem.* 2006; **49**(2): 534–553.
PubMed Abstract | **Publisher Full Text**

20. **Schrödinger Release 2016-3: Prime.** Schrödinger, LLC, New York, NY, 2016.

21. **https://www.pdc.kth.se/software/software/GROMACS/centos7/5.1.2/index.html**

22. Karplus M, McCammon JA: **Molecular dynamics simulations of biomolecules.** *Nat Struct Biol.* 2001; **9**(9): 646–52.
PubMed Abstract | **Publisher Full Text**

23. Carbó R, Leyda L, Arnau M: **How similar is a molecule to another? An electron density measure of similarity between two molecular structures.** *Int J Quantum Chem.* 1980; **17**(6): 1185–1189.
Publisher Full Text

24. Amat L, Carbó-Dorca R: **Use of promolecular ASA density functions as a general algorithm to obtain starting MO in SCF calculations.** *Int J Quantum Chem.* 2002; **87**(2): 59–67.
Publisher Full Text

25. Gironés X, Carbó-Dorca R: **Modelling Toxicity using Molecular Quantum Similarity Measures.** *QSAR Comb Sci.* 2006; **25**(7): 579–589.
Publisher Full Text

26. Carbó-Dorca R, Gironés X: **Foundation of quantum similarity measures and their relationship to QSPR: Density function structure, approximations, and application examples.** *QSAR Comb Sci.* 2006; **101**(1): 8–20.
Publisher Full Text

27. Morales-Bayuelo A, Torres J, Vivas-Reyes R: **Quantum molecular similarity analysis and quantitative definition of catecholamines with respect to biogenic monoamines associated: Scale alpha and beta of quantitative convergence.** *Int J Quant Chem.* 2012; **112**(14): 2637–2642.
Publisher Full Text

28. Morales-Bayuelo A, Vivas-Reyes R: **Topological model to quantify the global reactivity indexes as local in Diels–Alder reactions, using density function theory (DFT) and local quantum similarity (LQS).** *J Math Chem.* 2013; **51**: 125–143.
Publisher Full Text

29. Morales-Bayuelo A, Torres J, Baldiris R, *et al.*: **Theoretical study of the chemical reactivity and molecular quantum similarity in a series of**

30. derivatives of 2-adamantyl-thiazolidine-4-one using density functional theory and the topo-geometrical superposition approach. *Int J Quant Chem.* 2012; **112**: 2681–2687.
Publisher Full Text

30. Morales-Bayuelo A, Torres J, Vivas-Reyes R: **Hückel treatment of pyrrole and pentalene as a function of cyclopentadienyl using local quantum similarity index (LQSI) and the Topo-Geometrical Superposition Approach (TGSA).** *J Theo Comp Chem.* 2012; **11**(1): 223–239.
Publisher Full Text

31. Gironés; X, Robert D, Carbó-Dorca R: **TGSA: A molecular superposition program based on topo-geometrical considerations.** *J Comput Chem.* 2001; **22**(2): 255–263.
Publisher Full Text

32. Frisch MJG, Trucks W, Schlegel HB, *et al.*: **GAUSSIAN 09, Revision C.01,** Gaussian; Inc., Wallingford, 2010.
Reference Source

33. Beeke AD: **Density-functional thermochemistry. III. The role of exact exchange.** *J Chem Phys.* 1993; **98**: 5648.
Publisher Full Text

34. Lee C, Yang W, Parr RG: **Development of the Colle-Salvetti correlation-energy formula into a functional of the electron density.** *Phys Rev B.* 1988; **37**: 785.
PubMed Abstract | **Publisher Full Text**

35. Krishnan R, Binkley JS, Seeger R, *et al.*: **Self-consistent molecular orbital methods. XX. A basis set for correlated wave functions.** *J Chem Phys.* 1980; **72**: 650.
Publisher Full Text

36. R. Dennington, Inc: Wallingford, CT, 2008.

37. Malhotra V, Arteaga-Cortés LT, Clay G, *et al.*: **Mycobacterium tuberculosis protein kinase K confers survival advantage during early infection in mice and regulates growth in culture and during persistent infection: implications for immune modulation.** *Microbiology (Reading).* 2010; **156**(Pt 9): 2829–2841.
PubMed Abstract | **Publisher Full Text** | **Free Full Text**

38. Zuccotto F, Ardini E, Casale E, *et al.*: **Through the "gatekeeper door": exploiting the active kinase conformation.** *J Med Chem.* 2010; **53**(7): 2681–2694.
PubMed Abstract | **Publisher Full Text**

F1000Research

Open Peer Review

Current Peer Review Status: ✓

Version 1

Reviewer Report 24 February 2021

https://doi.org/10.5256/f1000research.31058.r78802

✓ **Hugo Fraga**
Faculdade de Medicina da Universidade do Porto - FMUP, Porto, Portugal

Although the scientific question is interesting - I don't understand how the question stated in the introduction: "what are the protein substrates of the STPKs?" can be directly answered by studying ATP competitive inhibitors. We already know ATP is a binder - what we don't know are the proteins that are targets for the kinases. Perhaps, by having specific inhibitors that would help in the identification of the targets but this is not stated in the introduction. Nevertheless, this does not reduce the interest of the study per se – to study the binding surface of putative kinase inhibitors is itself relevant. While this is a computational study, and the methodology and results look sound, I feel that some experimental data would be required to validate the exercise. It would be interesting to test if the residues identified – by mutating etc – do influence the IC50 of the compounds tested – but don't know how easy is to express the proteins and if the researchers have the know-how to perform such a task.

Something is missing in the sentence:
"The compounds to Pkn B have groups with electron withdraw- ing resonance effects, such as carbonyl, hydroxyl, amine and methoxy groups, with big rings central to its stabilization on the active site."

Is the work clearly and accurately presented and does it cite the current literature?
Yes

Is the study design appropriate and is the work technically sound?
Yes

Are sufficient details of methods and analysis provided to allow replication by others?
Yes

If applicable, is the statistical analysis and its interpretation appropriate?
I cannot comment. A qualified statistician is required.

Are all the source data underlying the results available to ensure full reproducibility?
Yes

Are the conclusions drawn adequately supported by the results?
Yes

Competing Interests: No competing interests were disclosed.

Reviewer Expertise: Tuberculosis, Drug Development

I confirm that I have read this submission and believe that I have an appropriate level of expertise to confirm that it is of an acceptable scientific standard.

Author Response 24 Feb 2021
Ph. D. Alejandro Morales-Bayuelo, Fundación UNiversitaria Tecnologico Comfenalco, Cartagena de Indias, Colombia

Ok, thank you very much by the sugestions. PKs (or PK domains within a larger protein) are generally made up of two lobes separated by a large cavity capable of including the substrate and a smaller cavity capable of including Adenosine TriphosPhate (ATP). The N-terminal lobe is mainly made up of β sheets and a conserved helix called the "C-helix". The C-terminal lobe is larger and is made up mostly of α-helices. In general, molecules that are designed with the intention of inhibiting PKs compete with ATP. For this reason, the inhibitors with higher activity has been selected inthis work for the PKs selected.

It has been reported that there is a relationship between the characteristics found at the ATP binding site and the pharmacology associated with this site. In the current work, a characterization of the 3D structures of the PKs involved in tuberculosis was made. To study these protein kinases, the components that make up the ATP binding site were also taken into account, such as the hinge zone residues, gatekeeper residue, presence or absence of the domain (DFG) and position of the glutamate residue conserved in the C-helix.

On the other hand, For the future, the experimental studies to extrapolate the conclusions are being consolidated. However, for the moment this study uses the experimental data of the activities and performs computational analyzes.

Best regards
_____
Alejandro Morales-Bayuelo.
Chemist.
Molecular Physical Chemistry Ph. D.
Molecular Physical-Chemistry Post-doctoral
Molecular Biophysics Post-doctoral
Academic Researcher.
Cartagena de Indias, Colombia.

The benefits of publishing with F1000Research:

- Your article is published within days, with no editorial bias

- You can publish traditional articles, null/negative results, case reports, data notes and more

- The peer review process is transparent and collaborative

- Your article is indexed in PubMed after passing peer review

- Dedicated customer support at every stage

For pre-submission enquiries, contact research@f1000.com

F1000Research